Staggering of Subunits in NMDAR Channels

Alexander I. Sobolevsky, LeeAnn Rooney, and Lonnie P. Wollmuth
Department of Neurobiology and Behavior, State University of New York at Stony Brook, Stony Brook, New York 11794-5230 USA

ABSTRACT   Functional *N*-methyl-D-aspartate receptors (NMDARs) are heteromultimers formed by NR1 and NR2 subunits. The M3 segment, as contributed by NR1, forms the core of the extracellular vestibule, including binding sites for channel blockers, and represents a critical molecular link between ligand binding and channel opening. Taking advantage of the substituted cysteine accessibility method along with channel block and multivalent coordination, we studied the contribution of the M3 segment in NR2C to the extracellular vestibule. We find that the M3 segment in NR2C, like that in NR1, contributes to the core of the extracellular vestibule. However, the M3 segments from the two subunits are staggered relative to each other in the vertical axis of the channel. Compared to NR1, homologous positions in NR2C, including those in the highly conserved SYTANLAAF motif, are located about four amino acids more externally. The staggering of subunits may represent a key structural feature underlying the distinct functional properties of NMDARs.

INTRODUCTION

Glutamate, the major excitatory neurotransmitter in the brain, activates three distinct types of ionotropic glutamate receptors (GluRs), specifically *N*-methyl-D-aspartate (NMDA), α-amino-3-hydroxy-5-methyl-4-isoxazolepropionate (AMPA), and kainate (KA) receptor subtypes (Hollmann and Heinemann, 1994). Each subtype displays a variety of unique molecular and biophysical properties that contribute to its prominence in synaptic physiology. Notable in this regard are NMDARs. Relative to other GluRs, NMDARs show very slow activation, deactivation, and desensitization kinetics. They also represent one of the most highly regulated ligand-gated ion channels (see Dingledine et al., 1999). Indeed, the activity of NMDAR channels is modulated by a variety of extracellular (e.g., Zn^{2+}, pH, Mg^{2+}, redox agents) and intracellular signals (e.g., Na^+, Ca^{2+}, Ca^{2+}/calmodulin, tyrosine kinases) and proteins (e.g., PSD-95). Even membrane tension (Paoletti and Ascher, 1994) and light (Leszkiewicz et al., 2000) alter NMDAR activity. These diverse gating and regulatory properties confer unto NMDARs considerable flexibility, contributing to their distinctive role in detecting and integrating pre and postsynaptic activity.

Functional NMDARs, in contrast to other GluR subtypes, are obligate heteromultimers, being formed by the NR1 and NR2 subunits. (At certain synapses, NR1 and NR3 may also form functional NMDARs (Chatterton et al., 2002).) In terms of the complexity of NMDAR function, the distinction between subunits is important because its diverse properties are invariably associated with a specific subunit, either NR1 or NR2. Hence, NMDAR channel opening requires the co-agonists glutamate and glycine with their binding domains located in the NR2 and NR1 subunits, respectively (Kuryatov et al., 1994; Hirai et al., 1996; Laube et al., 1997; Anson et al., 1998). Similarly, different forms of desensitization, modulation by intracellular and extracellular signals, and even properties related to the ion conduction pathway, such as Ca^{2+} permeation and channel block, are NR1 or NR2 subunit-specific (e.g., Burnashev et al., 1992; Krupp et al., 1998; Villarroel et al., 1998; Wollmuth et al., 1998; Kashiwagi et al., 2002; Vissel et al., 2002). Although the molecular basis of these properties can be linked to specific residues in a subunit, exchanges between subunits rarely confer a gain-of-function, indicating that the NMDAR subunits are not mirror images of each other. Nevertheless, the structural basis for the general distinction between the two subunits remains unknown.

The ion channel associated with NMDARs, like all other ion channels, consists of a water-filled pore divided into intracellular and extracellular vestibules by a narrow constriction. The intracellular vestibule is formed by the M2 loops from the two subunits (Kuner et al., 1996). The extracellular vestibule, as contributed by the NR1 subunit, is formed by residues on the N-terminal side of the M1 segment (pre-M1), the C-terminal part of the M3 segment, and the N-terminal part of the M4 segment (Beck et al., 1999). These domains, however, do not make equivalent contributions with M3 forming the core of the extracellular vestibule leading up to the channel's narrow constriction and pre-M1, M4, and regions C-terminal to M3 forming more superficial parts (Sobolevsky et al., 2002). Indeed, the NR1 M3 segment contains deep sites for trapping blockers with much of the voltage drop occurring over it, indicating that it represents a key structural domain. The M3 segment also undergoes extensive remodeling during the process of channel gating, reflecting its critical role in coupling ligand binding to channel opening (Sobolevsky et al., 2002; Jones et al., 2002). At present, the contribution of the NR2 subunit to the extracellular vestibule is unknown. Because of its structural and functional importance in NR1, we focused on the M3

Address reprint requests to Dr. Alexander I. Sobolevsky, Department of Neurobiology and Behavior, State University of New York at Stony Brook, Stony Brook, NY 11794-5230. Tel.: 631-632-4406; Fax: 631-632-6661; E-mail: asobolevsky@notes2.cc.sunysb.edu.

segment in NR2C to contrast the contribution of the subunits to channel structure.

To address the contribution of the NR2C M3 segment to the extracellular vestibule, we took advantage of the substituted cysteine accessibility method (SCAM) along with channel block and multivalent coordination. We find that the accessibility patterns of the M3 segments in the two subunits are comparable, with several notable exceptions. Surprisingly, however, based on the pattern of accessibility, the voltage dependence of reaction rates, and protection/facilitation by channel blockers, we find that the subunits are staggered relative to each other in the vertical axis of the channel with positions in NR2C located more externally than homologous ones in NR1. This staggering model of the subunits is supported by the coordination of Cu^{2+} by cysteines occupying nonhomologous positions. This depth asymmetry may represent a key structural feature underlying the complex gating and regulatory properties of NMDAR channels and may account for the differential contribution of the two subunits to a variety of functional properties.

MATERIALS AND METHODS

Mutagenesis and expression

All experiments were performed with previously described expression constructs for wild-type NR1 and NR2C NMDAR subunits (Kuner et al., 1996; Beck et al., 1999). Cysteine substitutions in the NR2C subunit were generated by the megaprimer PCR method (Trower, 1996) using Pfu DNA polymerase (Stratagene, La Jolla, CA). All constructs were sequenced over the entire length of the replaced fragment. cRNA was transcribed and capped for each expression construct using SP6 RNA polymerase (Ambion Inc., Austin, TX) and examined electrophoretically on a denaturing agarose gel. RNA concentrations were determined by ethidium bromide stain of the gel relative to an RNA molecular weight marker. Dilutions of RNA (0.01–0.1 $\mu g/\mu l$) were prepared to achieve optimal expression. Wild-type and mutant NR1 and NR2C subunits were co-expressed in *Xenopus laevis* oocytes. Oocytes were prepared, injected, and maintained as described (Wollmuth et al., 1996; Sobolevsky et al., 2002). Recordings were made two to five days after injections.

Current recordings and data analysis

Whole-cell currents of *Xenopus* oocytes were recorded at room temperature (20–23°C) using two-electrode voltage-clamp (DAGAN TEVA-200A, DAGAN Corp., Minneapolis, MN) with PULSE software (WaveMetrics Inc., Lake Oswego, OR). Microelectrodes were filled with 3 M KCl, and had resistances of 1–4 MΩ. To minimize solution exchange rates, we used a narrow flow-through recording chamber with a small volume of ~70 μl.

The external solution consisted of (mM): 115 NaCl, 2.5 KCl, 0.18 $CaCl_2$, and 10 HEPES (pH 7.2, NaOH). When Ag^+ was the test reagent, the solution was the same except that NO_3^- salts were used. All agonists, reagents, and blockers were applied with the bath solution. The concentrations of glutamate and glycine were 200 μM and 20 μM, respectively.

Data analysis was done using Igor Pro (WaveMetrics, Inc.) and Microcal Origin 4.1 (Northampton, MA). For analysis and display, leak currents were subtracted from total currents. Results are presented as mean ± SEM An ANOVA or a Student's *t*-test was used to test for statistical differences.

The Tukey test was used for multiple comparisons. Significance was assumed if $p < 0.05$.

Chemical modification

NMDAR cysteine-substituted mutant channels were probed from the extracellular side of the membrane with Ag^+, multivalent ions, and methanethiosulfonate (MTS) reagents: 2-aminoethyl MTS (MTSEA), 2-(trimethylammonium)ethyl MTS (MTSET), and 3-(triethylammonium)propyl MTS (PTrEA). Solutions contained MTS reagents and Ag^+ were prepared, stored, and applied as described (Sobolevsky et al., 2002). MTS reagents were purchased from Toronto Research Chemicals, Inc. (Ontario, Canada). All other chemicals were obtained from Sigma (St. Louis, MO).

Steady-state reactions

Steady-state reactions were quantified at −60 mV (see Fig. 2 *A*). Baseline glutamate-activated current amplitudes (I_{pre}) were established by four consecutive 15-s applications of glutamate separated by 105-s washes in glutamate-free solution. During the fifth glutamate application (90 s), an MTS reagent (2 mM), Ag^+ (1 μM), or a multivalent cation (see below) was applied for 60 s. After the test reagent application, current amplitudes (I_{post}) were determined again using at least four glutamate applications. The change in the current amplitude, expressed as a percentage, was calculated as $(1 - I_{post}/I_{pre}) \times 100$. The washout interval between the end of the reagent application and the first test glutamate application ranged from 1.25 to 5 min.

Reaction rates

Reaction rates, measured at −60 mV except for Fig. 4, were determined by using a "pulsive" protocol: the rate of change in current amplitudes was determined by applying a reagent for a specified amount of time and measuring current amplitudes before and after this application (e.g., Fig. 3). Compared to the "continuous" protocol used for NR1 (Sobolevsky et al., 2002), the "pulsive" protocol has two advantages: 1) it avoids any reversible component in the kinetic analysis, and 2) allows a direct comparison of reaction rates measured in the presence of glutamate and in the presence of the channel blocker (e.g., Fig. 5) because the latter is done with "pulsive" protocol. Changes in current amplitudes were fitted with a single exponential:

$$I = I_\infty + (I_0 - I_\infty)\exp(-t/\tau) \tag{1}$$

where t is the cumulative time of exposure to the reagent, I is the current after t seconds of this exposure, I_0 is the initial current (at $t = 0$), I_∞ is the asymptotic current when the reaction is complete, and τ is the time constant. The apparent second-order rate constant for chemical modification, k, was related to τ by:

$$k = 1/(\tau[C]) \tag{2}$$

where $[C]$ is the concentration of the MTS reagent.

Accurate measurements of reaction rates require the rate of solution exchange faster than the rate of the reaction itself. We adjusted the time of complete solution exchange, estimated from the kinetics of open tip responses, to ~10 s. MTS concentrations were selected such that τ was on the order of 50–200 s. Current "run-down" was tested in the absence of MTS reagents during a time interval needed to characterize τ and was always <10%.

FIGURE 1 Sequence alignment of the M3 segments in NMDAR NR1 and NR2C subunits. Schematic representation of an NMDAR subunit (NR1 or NR2) is shown. Open boxes illustrate hydrophobic segments M1, M2, M3, and M4. Below is the enlarged region encompassing the M3 segment. Positions in NR2C substituted with cysteines in the present study are indicated (CC. . . CC). The highly conserved SYTANLAAF motif is highlighted in gray. The three-digit numbers denote the position in the mature protein. Alternatively, amino acids are numbered relative to the first position (S) in the SYTANLAAF motif. Based on the membrane topology of GluR subunits, higher numbered positions are located more externally.
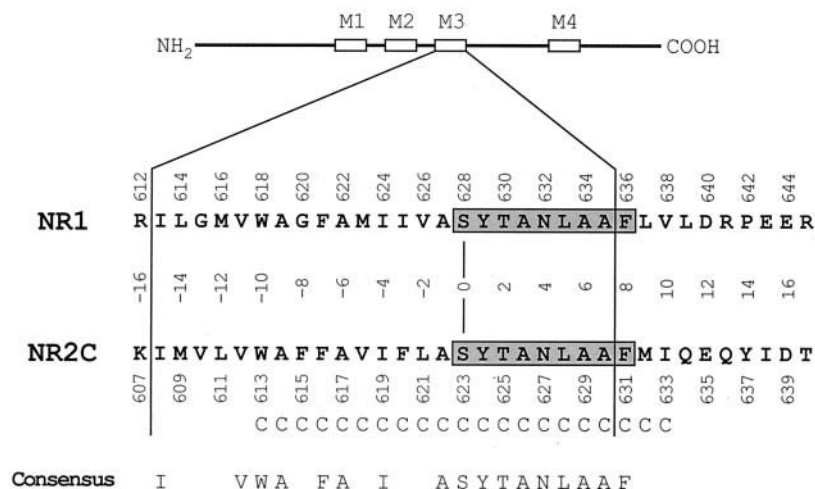
The voltage-dependence of k was analyzed according to the following equation:

$$k = k_0 \exp(-z\delta F V_h / RT) \tag{3}$$

where V_h is the holding potential, k_0 is the apparent second-order rate constant for modification at $V_h = 0$, and $z\delta$ is the fraction of the transmembrane electric field the MTS reagent passes to reach the exposed cysteine. F, R, and T have their usual meaning. To derive $z\delta$, we rearranged Eq. 3:

$$-(RT/F) \operatorname{Ln} k = A + z\delta V_h \tag{4}$$

where A is $-(RT/F)\operatorname{Ln} k_0$, and fitted Eq. 4 to plots of $-(RT/F)\operatorname{Ln} k$ against V_h.

Multivalent reactions

To test for multivalent coordination we used a steady-state protocol as outlined above, applying various multivalent cations for 60 s in the continuous presence of glutamate and monitoring current amplitudes before and after this test application. The multivalents tested, at an initial screening concentration of 0.1–1 mM, include Cd^{2+}, Co^{2+}, Cu^{2+}, Fe^{2+}, Mn^{2+}, Ni^{2+}, Sr^{2+}, Zn^{2+}, As^{3+}, Fe^{3+}, and La^{3+}. Some of these substances (e.g., Fe^{3+} and La^{3+}) produced a nonspecific inhibition, irreversibly inhibiting currents through wild-type channels, and we did not explore them further. The alternative and most common effect for wild-type and the cysteine-substituted mutant channels was a transient inhibition of the glutamate-activated current that occurred during the application of the multivalent ion and that was completely or nearly completely reversed upon its removal (I_{post} was at minimum 85% of I_{pre}). Because these test multivalents did not produce irreversible effects, we did not calculate their free concentrations. However, Cu^{2+} did produce a specific effect (see Fig. 6). Based on adding 100 μM Cu^{2+} to the external solution, the concentrations of free Cu^{2+} (11 nM), glutamate (108 μM), and glycine (7.7 μM) were computed as described previously (Vlachova et al., 1996) using stability constants for copper-glutamate ($K_1 = 7.85$, $K_2 = 6.55$) and copper-glycine ($K_1 = 8.12$, $K_2 = 6.91$) complexes (Sillen and Martell, 1964).

RESULTS AND DISCUSSION

Fig. 1 shows a sequence alignment of the M3 segment and regions C-terminal to it in the NR1 and NR2C subunits. Notable in this region is SYTANLAAF, the most highly

conserved motif in GluR subunits (Sprengel et al., 2001). Our major goal was to compare the relative contribution of the two subunits to the extracellular vestibule. For ease of comparison, we therefore referenced positions relative to the first one (S) in SYTANLAAF.

Residues within and C-terminal to the NR2C M3 segment were individually mutated to cysteine (Fig. 1). When co-expressed with the wild-type NR1 subunit in *Xenopus* oocytes, 16 of 21 cysteine-substituted NR2C mutants generated glutamate-activated currents comparable in amplitude to wild type, four (W-10C, Y+1C, L+5C, and F+8C) generated smaller currents, and one (N+4C) did not generate detectable current. However, co-expression of NR2C(N+4C) with wild-type NR2C and NR1 (1:1:2) gave glutamate-activated currents comparable in amplitude to wild type. These currents, in contrast to those in wild-type NR1-NR2C channels, were persistently altered by MTS reagents (e.g., Fig. 2 B), indicating that the cysteine-substituted subunit was incorporated into functional channels, presumably NR1-NR2C-NR2C(N+4C). For all cysteine-substituted mutant channels, leak currents were comparable in amplitude to that in wild type.

Accessibility of substituted cysteines in NR2C to MTS reagents

Fig. 2 A illustrates our approach to determining steady-state accessibility of substituted cysteines in the presence of glutamate. Glutamate-activated currents were recorded before (I_{pre}) and after (I_{post}) the application of the MTS reagent, MTSEA (2 mM, *thick line*), which was applied in the continuous presence of glutamate (*thin lines*). Fig. 2 B shows the mean percent change in current amplitudes before and after exposure to MTSEA. We considered a position accessible if I_{post} was significantly different from I_{pre} (*filled bars*). For accessible positions, MTSEA typically reduced
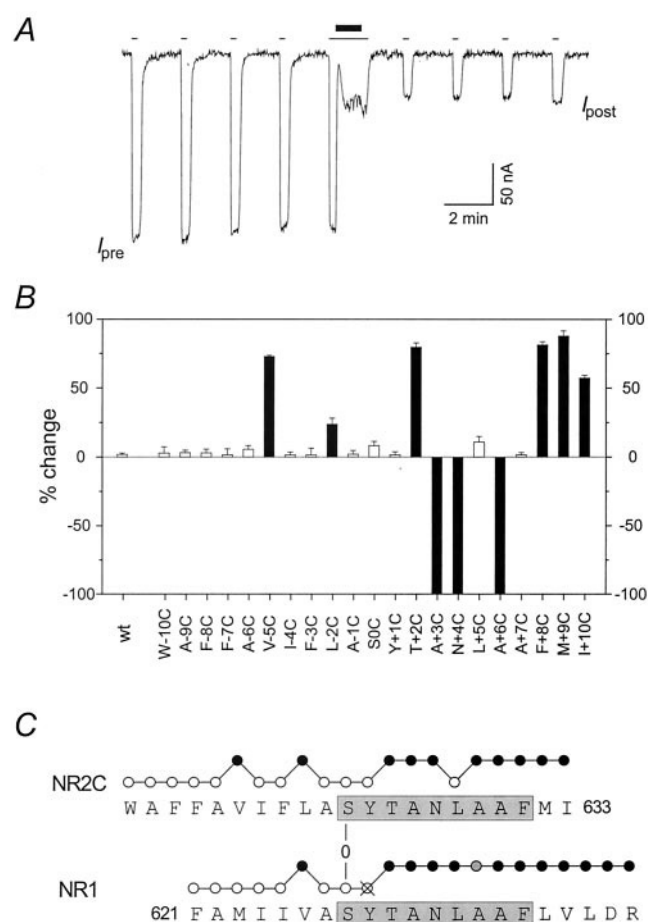
FIGURE 2 Accessibility of substituted cysteines in the NR2C subunit to MTS reagents. (*A*) Protocol to assay accessibility of substituted cysteines in the presence of glutamate using steady-state reactions (see Materials and Methods). The example shows whole-cell currents recorded from a *Xenopus* oocyte expressing NR1-NR2C(V-5C). Currents were elicited by glutamate (*thin lines*) at a holding potential (V_h) of -60 mV. MTSEA (2 mM, *thick line*) was applied for 60 s in the continuous presence of glutamate. (*B*) Mean percent change in current amplitudes measured before (I_{pre}) and after (I_{post}) exposure to MTSEA in the presence of glutamate. Up- and down-pointing bars indicate inhibition and potentiation, respectively ($n = 4$). Filled bars indicate a statistical difference between I_{post} and I_{pre}. For A+3C, N+4C, and A+6C, currents were potentiated by >100%. For N+4C, the mutant subunit was co-expressed with wild-type NR2C and NR1(1:1:2). (*C*) Binary representation of the accessibility of substituted cysteines to MTS reagents. A position is considered accessible (*filled circle*) if at least one of the MTS reagents, MTSEA, MTSET, or PTrEA, produced a significant alteration in glutamate-activated current. Other positions are represented as open circles. The NR1 results are from Beck et al. (1999). NR1(Y+1C) (*crossed circle*) does not produce functional channels. NR1(A+6C) (*gray circle*) exhibits a strong and irreversible inward current after MTS exposure.

current amplitudes, but in three instances, A+3C, N+4C, and A+6C, it strongly potentiated them.

The accessibility pattern of substituted cysteines in NR2C to the larger and permanently charged MTS reagents MTSET and PTrEA (data not shown) was similar to that for MTSEA, with two notable differences. First, for A+7, MTSEA did not alter glutamate-activated currents, whereas this position was accessible to MTSET and PTrEA. For example, MTSET produced a percent change of -113.3 ± 3.3 (mean $\pm$ SE, $n = 4$). However, MTSET, when applied to cells that had already been exposed to MTSEA, did not change glutamate-activated currents (% change $= 0.5 \pm 6.5$, $n = 5$), indicating that MTSEA produced a silent reaction with the cysteine substituted at A+7, covalently modifying the sulfhydryl group without affecting current flow. Second, position V-5 was accessible to MTSEA, but showed no reactivity to MTSET or PTrEA. Because MTSEA exists both in ionized and non-ionized forms, it could access the substituted cysteine at V-5C via the lipid phase. However, the modification rate of V-5C by MTSEA was strongly voltage-dependent (see below) and V-5C was accessible to Ag^+ (% change $= 55 \pm 5\%$, $n = 5$), a sulfhydryl specific reagent that is smaller than MTSEA but permanently charged. Therefore, the different reactivity of V-5C with various-sized MTS reagents more likely reflects steric constraints on accessibility.

In summary, 10 of 21 cysteines substituted in NR2C showed a reaction with various-sized MTS reagents. The interpretation of reactive and nonreactive positions is constrained by the assumptions of SCAM (Beck et al., 1999; Karlin and Akabas, 1998). Specifically, we assume that those positions that are reactive are exposed to the water interface and line the lumen of the channel. We also assume that nonreactive positions are buried in the interior of the protein, particularly when adjacent positions are accessible to the reagents. Correspondingly, based on the presumed membrane topology of GluR subunits, we assume that V-5 in NR2C represents the deepest exposed position in the extracellular vestibule as contributed by NR2C because five consecutive deeper positions (A-6 to W-10) were not accessible to any MTS reagent.

Fig. 2 *C* compares, in a binary fashion, the accessibility patterns for the M3 segment and regions C-terminal to it in NR1 and NR2C. In general, the accessibility patterns for the two subunits are comparable, suggesting that they may share a common secondary structure. Although any detailed structural inference is limited (see Karlin and Akabas, 1998), the accessibility of every third/fourth residue in the deep part of both subunits is consistent with an α-helical conformation. More external parts of the subunits, starting at T+2 in SYTANLAAF, have lengthy regions of accessible positions, with NR2C(L+5) being the only exception. This high degree of accessibility could reflect that a presumed α-helical conformation of the deep part of M3 changes at T+2 to an extended structure more externally. Alternatively, the entire M3 segment could be α-helical, with the regions of consecutive accessibility reflecting a high degree of state-dependent flexibility.

Although the accessibility pattern for both subunits is comparable, it does show one surprising difference deep in

the pore (Fig. 2 *C*). For both subunits, position -2 is accessible. However, this position is the deepest one in NR1, whereas for NR2C an additional and presumably deeper position, -5, is also accessible. The accessibility of an additional deep position in NR2C suggests that the M3 segments in the two subunits may not share a common alignment in the vertical axis of the channel.

To test the hypothesis that the NMDAR subunits are staggered, we characterized in detail reaction rates for six selected positions in NR2C under various conditions (Figs. 3-5) and compared these results to previous ones obtained for NR1 (Sobolevsky et al., 2002). These NR2C positions—V-5, L-2, T+2, N+4, A+7, M+9—were selected because they encompass the region of substituted cysteines, and mutant channels containing them show large current amplitudes. For each position we typically used as a test MTS reagent (MTSEA, MTSET, or PTrEA), the one that produced the greatest percent change in steady-state accessibility experiments. For positions located outside the transmembrane electric field (Fig. 4), we preferentially used permanently charged MTS reagents (MTSET or PTrEA) to ensure that the reaction occurred via the water-filled pore.

Modification rate of cysteine-substituted NMDAR channels in the presence of glutamate

Fig. 3 *A* illustrates our protocol to measure modification rates in the presence of glutamate. An MTS reagent (*thick line*), in this case PTrEA, was applied five times in the presence of glutamate (*thin lines*). Glutamate-activated current amplitudes, plotted as a function of the cumulative time of MTS exposure, give the time course of chemical modification (Fig. 3 *B*). The time constant of the fitted exponential to these plots defines the apparent second-order rate constant for chemical modification in the presence of glutamate, k (Eq. 2).

Fig. 3 *C* summarizes mean reaction rates in the presence of glutamate for the six selected NR2C positions. These rates varied widely, but this variability is similar to that observed for NR1 positions (Sobolevsky et al., 2002) and probably reflects multiple factors that can affect k, including steric constraints, local electric field, local hydrophobicity, and orientation of the reactive groups. The most notable difference between the subunits is that in general, reaction rates for NR2C are much slower than those for NR1. Indeed, for NR2C, k was never greater than 10^3 M^{-1} s^{-1}, whereas for NR1, only two of seven positions tested (N+4 and L+5) had $k < 10^3$ M^{-1} s^{-1}. In part, this difference may reflect the larger size of the test MTS reagent (MTSET or PTrEA instead of MTSEA), but it could also be due to a differential arrangement of the NR1 and NR2C subunits relative to the central axis of the pore.
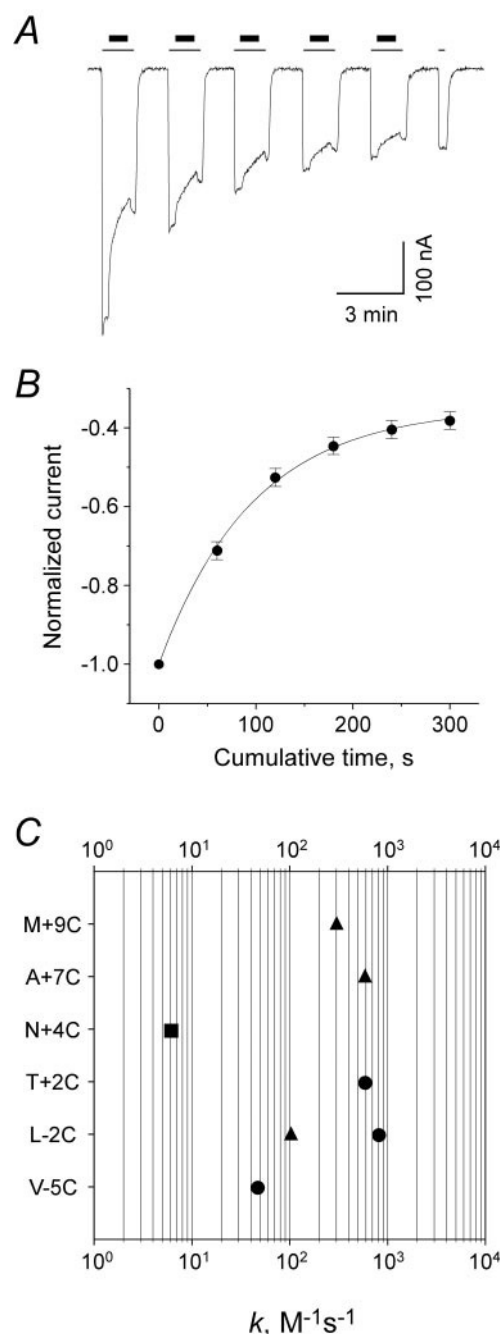

FIGURE 3   Modification rate of exposed cysteines in the presence of glutamate. (*A*) Pulsive protocol to assay modification rates in the presence of glutamate. The example shows NR1-NR2C(L-2C). V_h was -60 mV. The PTrEA application (100 μM, *thick line*, 1 min) was started 15 s after the beginning and finished 15 s before the end of the glutamate (*thin line*) application. The cell was washed for 1.5 min between glutamate applications. Current amplitudes, defining the time course of cysteine modification (*B*), were measured during the first 15 s of each glutamate exposure. (*B*) Normalized glutamate-activated current amplitudes as a function of cumulative time of PTrEA exposure. Points represent the average of six cells. Data are fitted by a single exponential function ($\tau = 103 \pm 6$ s). (*C*) Apparent second-order rate constants, k, for chemical modification of substituted cysteines in the presence of glutamate. These constants were derived using Eq. 2 and are shown as circles for MTSEA, squares for MTSET, and triangles for PTrEA. SEM values are smaller than the symbol size ($n = 4$).
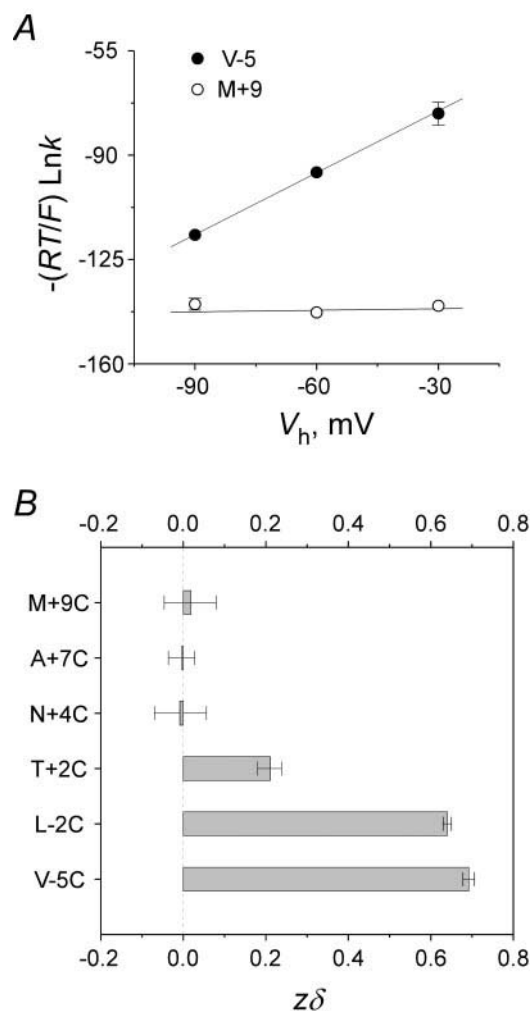
FIGURE 4 Voltage-dependence of the modification rate. (*A*) Apparent second-order rate constant for chemical modification, expressed in a logarithmic form ($-(RT/F)*\text{Ln } k$), as a function of the holding membrane potential, V_h. The examples show V-5C (*filled circles*, MTSEA) and M+9C (*open circles*, PTrEA). The k values were estimated using the same protocol as that illustrated in Fig. 3 *A*. The error bars are not shown if smaller than the symbol size. The straight lines through the points are fits with Eq. 4 with their slopes giving $z\delta$: 0.69 ± 0.01 for V-5C and 0.02 ± 0.06 for M+9C. (*B*) Mean $z\delta$ estimated using the method described in *A*. The data are for MTSEA (V-5, L-2, and T+2), MTSET (N+4), and PTrEA (A+7 and M+9). A minimum of four cells was recorded at each potential.

Voltage dependence of modification rates

One approach we have used to characterize the relative positioning of exposed residues in the NR1 subunit was to measure reaction rates as a function of voltage (Sobolevsky et al., 2002). To study the voltage dependence of reaction rates in NR2C, we carried out experiments such as those illustrated in Fig. 3 at different membrane potentials, V_h. Fig. 4 *A* shows two examples of the rate constants, expressed in a logarithmic form ($-(RT/F)*\text{Ln } k$), as a function of V_h. For V-5, the rate constants were strongly voltage-dependent, getting faster at more negative potentials. In

contrast, for M+9, the rate constants were voltage-independent. The slope of the fitted line (Eq. 4) to these plots gives an estimation of the fraction of the transmembrane electric field, $z\delta$, the MTS reagent passes to reach the exposed cysteine. Fig. 4 *B* summarizes the $z\delta$ values for the six selected positions. The strongest voltage dependence was observed for V-5 ($z\delta = 0.69 \pm 0.01$) and L-2 ($z\delta = 0.64 \pm 0.01$). Position T+2 ($z\delta = 0.21 \pm 0.03$) showed a much weaker voltage dependence. However, the reaction rates for N+4, A+7, and M+9 were voltage-independent. Thus, the voltage dependence of reactivity is strongest for the presumed deepest positions and becomes weaker as one moves more externally.

Clearly, the $z\delta$ values do not necessarily correspond to any physical distance, and various local factors could affect them differently for the two subunits. Nevertheless, taking into account the consistency of the overall voltage dependence—it drops uniformly from presumed deep to external positions in both subunits—we believe that the transmembrane electric field drops synchronously for both NR1 and NR2C. We therefore assume that the $z\delta$ values for NR2C (Fig. 4 *B*) and NR1 (Sobolevsky et al., 2002) measured using MTSEA gives an approximate index of the relative location of the exposed positions in the extracellular vestibule.

Based on $z\delta$ values for MTSEA, we aligned positions in NR1 and NR2C along the central axis of the pore in a one-to-one manner (Fig. 7). The two deepest exposed positions, NR1(V-2) and NR2C(V-5), both show the strongest voltage dependence (0.71 and 0.69, respectively) and hence are placed at the same approximate vertical level. A similar asymmetrical alignment is required for more external residues including A+3/N+4 in NR2C and A+7/F+8 in NR1, which are the first positions showing a reactivity that is voltage-independent. Thus, the alignment based solely on the voltage dependence of reactivity requires a staggering of the subunits with homologous positions in NR2C located about four amino acids more externally (Fig. 7). The error in estimating the magnitude of the subunit asymmetry is approximated by the mean errors in estimating $z\delta$ values for both subunits (~ 0.04). Because 71% of the transmembrane electric field drops over the nine consecutive amino acids (from V-2 to A+7 in NR1 or from A-6 to A+3 in NR2C) and assuming a linear relationship between $z\delta$ and distance, this error estimate leads to an uncertainty of 0.6 in the positioning of residues in NR2C relative to those in NR1. With this analysis, the magnitude of the staggering is 4.0 ± 0.6 residues. Assuming the M3 segments are α-helical, this staggering corresponds to 1.11 ± 0.15 turn or 6.0 ± 0.8 Å length of an α-helix.

In the model shown in Fig. 7, the $z\delta$ isolines become closer together for more externally located positions. This may reflect that 1) the deep part of M3 is α-helical but changes to an extended region more externally, or, alternatively, that 2) the electric field in the NMDAR pore is not

uniform. At present neither alternative can be ruled out, but other work supports the idea of a non-uniform electric field in NMDAR channels (Subramaniam et al., 1994; Antonov et al., 1998; Sobolevsky et al., 1999).

Protection of exposed cysteines by 9-aminoacridine

Sequential or "foot-in-the-door" blockers are a class of open channel blockers that prevent channel closure when they occupy the pore presumably because of their large size (Antonov et al., 1998; Sobolevsky et al., 1999). In NR1, we examined the reactivity of MTS reagents with exposed positions in the presence of one such sequential blocker, 9-aminoacridine (9-AA), and found a distinct pattern of reactivity: 9-AA protected from reaction positions deep in the pore but facilitated the reactions of more intermediate positions (Sobolevsky et al., 2002). We do not know the basis of this facilitating action, but it may reflect that 9-AA increases the channel open probability. Nevertheless, because of this distinct pattern of protection/facilitation, we took advantage of 9-AA as an additional tool to contrast the spatial positioning of the M3 segments in the NMDAR subunits.

To assay modification rates of NR2C-substituted cysteines in the presence of 9-AA, we used the same protocol as that described previously for NR1 (see Fig. 7, Sobolevsky et al., 2002). After a 15-s test glutamate application, glutamate and 9-AA (200 μM) were co-applied for 15 s. Glutamate was then removed, and 1 min later, MTS reagent was applied for 1 min in the continuous presence of 9-AA. After removal of MTS reagent, the cell was bathed an additional 15 s in 9-AA, and then was washed for 1.25 min before the next test glutamate application. One notable feature of this protocol is that we applied MTS reagents in the presence of 9-AA but in the absence of glutamate. However, because 9-AA locks NMDAR channels in the open state (Benveniste and Mayer, 1995; Sobolevsky, 1999), we compared the rate constants measured in the presence of 9-AA, $k_{9\text{-AA}}$, to those obtained in the presence of glutamate, k.

Fig. 5 contrasts $k_{9\text{-AA}}$ (*open symbols*) to k (*solid symbols*, from Fig. 3 *C*) for the six selected positions. For the deepest positions, V-5 and L-2, $k_{9\text{-AA}}$ was decreased by >10-fold compared to k, indicating that 9-AA provides protection from reaction with the MTS reagent. However, reaction rates for positions T+2 and N+4 were faster or facilitated in 9-AA relative to k. The most external position, M+9, also showed a decrease in reactivity in 9-AA. This protection presumably reflects that, as has been proposed previously (Sobolevsky and Koshelev, 1998; Sobolevsky, 1999), another open-channel blocking site exists that is located outside of the transmembrane electric field. Nevertheless, taking into account the voltage dependence of reactivity, the pattern of protection provided by 9-AA supports the idea
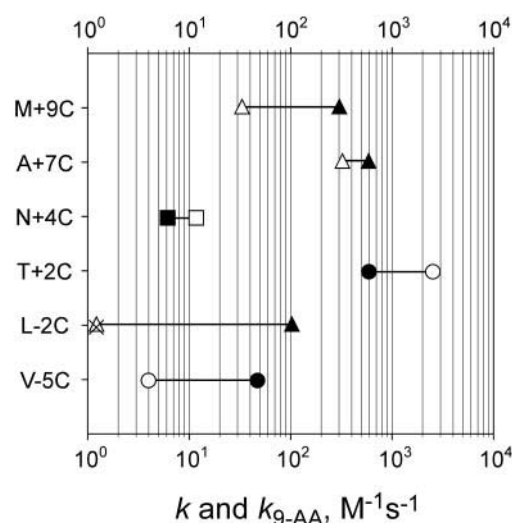

FIGURE 5 Protection of exposed cysteines by 9-aminoacridine. The second-order rate constants for modification of cysteines in the presence of 9-aminoacridine (9-AA) ($k_{9\text{-AA}}$) and in the presence of glutamate (k from Fig. 3 *C*) are shown as open and solid symbols, respectively. The protocol used to assay the protection of exposed cysteines by 9-AA is the same as described (Sobolevsky et al.; 2002). The rate constants are for MTSEA (*circles*), MTSET (*squares*), or PTrEA (*triangles*). Reaction rate for L-2C in the presence of 9-AA (*crossed triangle*) could not be determined properly because it required high concentrations of PTrEA (2 mM), which had nonspecific effects on membrane currents. This rate was not faster than 1 M^{-1} s^{-1}, but was assigned this value. SEM are smaller than the symbol size ($n = 4$).

that M3 in NR2C, like that in NR1, forms the core of the extracellular vestibule.

To compare the effects of 9-AA on positions in NR1 and NR2C, we overlaid the alignment in Fig. 7, based initially on the voltage dependence of reactivity, with the $k/k_{9\text{-AA}}$ ratio (*left* and *right panels*, respectively). In this model, the two deepest positions in NR1 and NR2C showed the greatest protection, with the most strongly protected positions, NR1(T+2) and NR2C(L-2), ($k/k_{9\text{-AA}} > 100$) located at the same level. Similarly, position T+2 shows the strongest facilitation in NR2C and lines up with corresponding facilitating positions in NR1 (L+5 and A+7). The correspondence between protection/facilitation and aligned positions diverges in only one instance: NR1(F+8) is protected, whereas NR2C(N+4) shows facilitation. However, neither effect is strong, and the small difference may reflect a nonperfect vertical alignment of the subunits and/or a preferred orientation of 9-AA in the pore relative to one of the subunits. In any case, the protection/facilitation pattern provided by 9-AA lends further support to the staggering model shown in Fig. 7.

Copper coordination by cysteines substituted at nonhomologous positions in NR1 and NR2C

Cysteine, along with histidine and methionine side chains, can coordinate metals in proteins (Holm et al.,

1996). Correspondingly, based on the vertical alignment shown in Fig. 7, one would anticipate that aligned positions containing substituted cysteines would preferentially coordinate multivalent cations. A caveat of these experiments is that a negative outcome does not rule out that positions are aligned, either homologous or nonhomologous, because the substituted cysteines may be in close proximity but are not oriented properly to coordinate the ion.

To test possible coordination, we applied different divalent (Cd^{2+}, Co^{2+}, Cu^{2+}, Fe^{2+}, Mn^{2+}, Ni^{2+}, Sr^{2+}, Zn^{2+}) or trivalent (As^{3+}, Fe^{3+}, La^{3+}) metal cations to channels formed by the NR1 and NR2C subunits, both containing substituted cysteines (see Materials and Methods). We tested all possible pairs between the three deepest exposed positions in NR1 (V-2, T+2, and N+4) and NR2C (V-5, L-2, and T+2), a total of nine different subunit combinations. All pairs generated glutamate-activated currents comparable in amplitude to wild-type channels, with two exceptions, NR1(T+2C)-NR2C(V-5C) and NR1(T+2C)-NR2C(T+2C), which produced currents too small to be reliably analyzed. Of all the multivalents tested on the different subunit combinations, only Cu^{2+} and only on a specific subunit combination (Fig. 6) produced a persistent inhibition of glutamate-activated currents that was >15%.

In wild-type NR1-NR2C channels, 100 μM Cu^{2+} (11 nM free Cu^{2+}, *open box*) applied in the presence of glutamate-attenuated current amplitudes, an effect that rapidly reversed upon its removal (Fig. 6 *A*, *left panel*). This transient inhibition by Cu^{2+} is comparable to that found in cultured hippocampal neurons under similar conditions (Vlachova et al., 1996). In contrast, Cu^{2+} strongly and irreversibly inhibited currents through NR1(T+2C)-NR2C(L-2C) channels (Fig. 6 *A*, *right panel*). Indeed, as summarized in Fig. 6 *B*, current amplitudes following the Cu^{2+} application in the double mutant were reduced by ~80% (% change = 80 ± 2, $n = 6$) compared to no persistent change in wild type (% change = 3 ± 2, $n = 6$). For channels containing only a single cysteine-substituted subunit, NR1(T+2C)-NR2C or NR1-NR2C(L-2C), no persistent inhibition by Cu^{2+} occurred (% change was 1 ± 3, $n = 5$, and 3 ± 2, $n = 5$, respectively).

The strong effect on NR1(T+2C)-NR2C(L-2C) channels suggests that the substituted cysteines coordinate Cu^{2+}. To test this idea, we applied the dithiol compound 2,3-dimercapto-1-propanesulfonate (DMPS, 1 mM) to Cu^{2+}-inhibited NR1(T+2C)-NR2C(L-2C) channels for 1 min (data not shown). DMPS, by using its two vicinal thiols, can displace protein ligands and release coordinated substances, as it does with arsenical reagents and Cd^{2+} in nicotinic acetylcholine receptors and K^+ channels (Loring et al., 1992; Liu et al., 1996, 1997). Supporting the idea of Cu^{2+} coordination by substituted cysteines, DMPS induced a recovery of
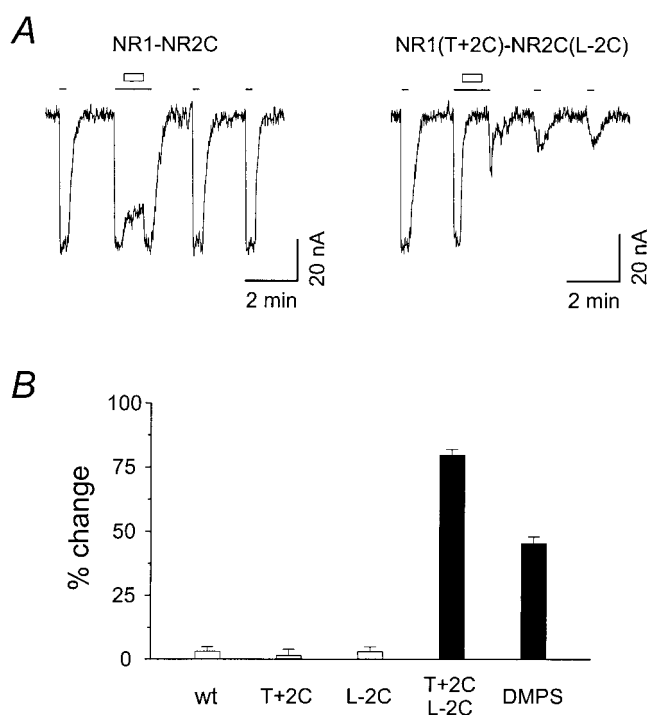

FIGURE 6 Copper coordination of substituted cysteines in the NR1 and NR2C subunits. (*A*) Steady-state protocol to assay the effect of Cu^{2+} on glutamate-activated currents. Cu^{2+} (100 μM, *open box*) was applied for 60 s in the presence of glutamate (*thin lines*). The examples show wild-type NR1-NR2C and NR1(T+2C)-NR2C(L-2C) channels. The estimated concentration of free Cu^{2+} was 11 nM (see Materials and Methods). (*B*) Mean percent change in current amplitudes measured before (I_{pre}) and after (I_{post}) exposure to Cu^{2+}. Subunit combinations shown include (*from left to right*): wild-type, NR1(T+2C)-NR2C, NR1-NR2C(L-2C), and NR1(T+2C)-NR2C(L-2C). For the DMPS condition, NR1(T+2C)-NR2C(L-2C) channels, which had already been exposed to Cu^{2+} (100 μM, 60 s), were exposed for 60 s to 1 mM DMPS. In this instance, I_{pre} and I_{post} correspond to the current amplitudes measured before Cu^{2+} and after DMPS treatments, respectively. Filled bars indicate a statistical difference between I_{post} and I_{pre} ($n > 5$).

almost half of the glutamate-activated current inhibited by Cu^{2+} (Fig. 6 *B*, % change = 45 ± 3, $n = 6$).

The coordination of Cu^{2+} by substituted cysteines at T+2 in NR1 and L-2 in NR2C is consistent with the idea that these nonhomologous positions are located in close proximity. In addition, this coordination must occur between cysteines substituted in different subunits, because it does not occur in channels containing only one mutated subunit. Hence, at least two cysteines, one from NR1 and one from NR2C, should participate in this coordination. Cu^{2+} can be coordinated via a number of effective geometries (tetrahedral, octahedral, square planar, square pyramidal, trigonal bipyramidal) with a maximal distance of ~3.6 Å between Cu^{2+} and thiolate in cysteine (Holm et al., 1996), suggesting that the maximal distance between the two coordinating cysteines should be <7.2 Å. Still, it is difficult to say more about the geometry and energy of this

FIGURE 7 Schematic representation of staggering of the NMDAR subunits. Amino acid residues in NR1 or NR2C are aligned along the central axis of the channel pore. Parts of the NR1 and NR2C M3 segment and adjacent region forming the core of the extracellular vestibule are shown. Filled ellipses indicate positions exposed to the lumen of the channel. The SYTANLAAF motif is shown in gray. Thin horizontal lines indicate the apparent fraction of the membrane voltage ($z\delta$) experienced by MTSEA reaching the substituted cysteine at the corresponding depth in the channel. The black circle in the center illustrates coordination of Cu^{2+} by cysteines substituted at positions NR1(T+2) and NR2C(L-2). Extreme left and right panels show the ratio k/k_{9-AA}, which summarizes the effect of 9-AA on chemical modification of substituted cysteines. The values for NR2C are shown in Fig. 5, whereas those for NR1 are taken from Fig. 7 of Sobolevsky et al. (2002). Bars pointing away from ($k/k_{9-AA} > 1$) or toward ($k/k_{9-AA} > 1$), the central axis of the pore, indicate protection and facilitation, respectively. For NR1(T+2) and NR2C(L-2), k/k_{9-AA} is >100, and for NR1(L+5) and NR1(A+7), it is <0.1.
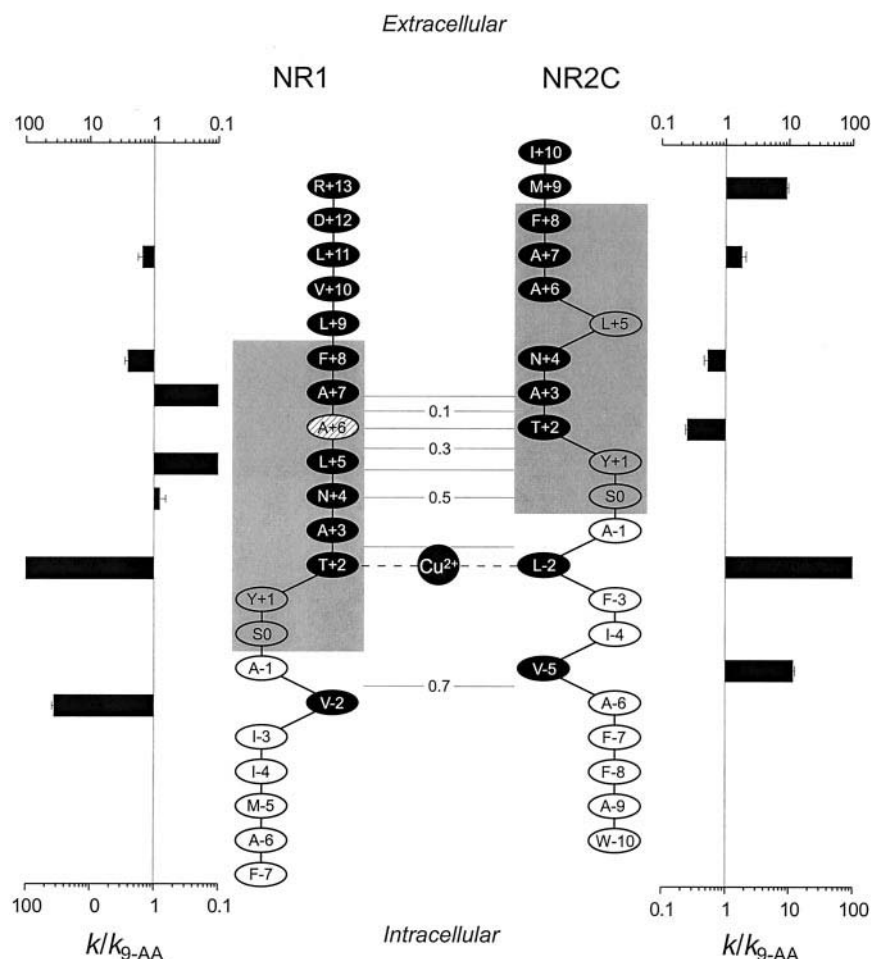
Cu^{2+} coordination because we do not know the exact number of cysteines involved (two or more) and the number (four or five) and arrangement of NMDAR subunits in the channel (e.g., 1-2-1-2 or 1-1-2-2 for tetramer). This issue is further complicated by the fact that backbone carbonyls can also be coordinating ligands (Holm et al., 1996) and that multiple copper ions can participate in coordination (Solomon et al., 1996). Nevertheless, the close proximity of NR1(T+2) and NR2C(L-2) suggested by experiments with Cu^{2+} strongly supports the staggering model illustrated in Fig. 7.

Staggering of the NMDAR NR1 and NR2C subunits

Our results indicate that the M3 segment in the NR2C subunit forms the core of the extracellular vestibule, like that in NR1. However, we also find that the M3 segments from the two subunits make distinct structural contributions to the pore. Indeed, based on numerous lines of evidence—the accessibility of substituted cysteines (Fig. 2), the voltage dependence of modification rates (Fig. 4), protection/facilitation by 9-AA (Fig. 5), and Cu^{2+} coordination (Fig. 6)—

the M3 segments are arranged such that positions in NR2C are located about four amino acids more externally than homologous ones in NR1 (Fig. 7). This staggering suggests that the M3 segments in the two subunits are offset by a single turn in a presumed α-helical conformation.

An asymmetrical positioning of the reentrant pore loops was found previously in voltage-gated Ca^{2+} and Na^+ channels (Yang et al., 1993; Chiamvimonvat et al., 1996) and in NMDAR channels (Kuner et al., 1996; Wollmuth et al., 1996). In NMDAR channels, however, the staggering proposed for the reentrant M2 loops is small, less than a single residue. Supporting this idea, cysteines substituted for the N-site asparagines in NR1 and NR2C are located in close enough proximity to coordinate Zn^{2+} with nanomolar affinity (Amar et al., 2001). Because the M2 loops share a very low sequence identity (18.5%; 5 of 27 residues), the small M2 loops asymmetry could reflect a local structural difference. In contrast, the M3 segments for the NR1 and NR2C subunits share a 70% identity (16 of 23 residues; Fig. 1) with SYTANLAAF representing the most highly conserved motif in GluR subunits. Given this high sequence similarity and the fact that M3 represents a transmembrane domain, it seems unlikely that the staggering of the M3

segments reflects a local structural difference. Rather, an asymmetrical positioning of subunits may be a fundamental principle of pore-forming domains in NMDAR channels and may represent a global structural feature of NMDAR subunits.

In NMDAR channels, and presumably in other GluR subtypes, the M3 segment represents the major transmembrane segment lining the pore. In other ligand- and voltage-gated ion channels, homologous positions in pore-forming transmembrane segments are generally believed to be at the same vertical level. Such a homologous positioning is most obvious for the K^+ channel KcsA, for which a crystal structure exists (Doyle et al., 1998). In contrast to NMDARs, however, KcsA channels are formed by identical subunits. Still, even for ion channels requiring heteromultimeric assemblies, such as $GABA_A$ and nicotinic acetylcholine receptor channels, homologous positions in the pore-forming domains (M2 segment) are approximately aligned in the vertical axis of the channel (e.g., Horenstein et al., 2001; Karlin, 2002). Thus, the staggering of NMDAR subunits—especially the magnitude of them—may represent a distinctive structural feature.

The M3 segment is a key transduction element coupling the conformational change in the ligand-binding domain to channel opening in GluR channels (Kohda et al., 2000; Sobolevsky et al., 2002; Jones et al., 2002). In NMDARs, channel opening requires binding of the co-agonists glutamate and glycine, the binding sites of which are associated with the NR2 and NR1 subunits, respectively. These two agonists, however, have very different effects on channel activation kinetics (Banke and Traynelis, 2001), suggesting that the conformational changes coupling ligand binding to channel opening in the two subunits are fundamentally different. The staggering of the subunits, by placing different constraints on the molecular motions during gating, may represent one mechanism underlying this gating asymmetry.

The extracellular vestibule is an important functional domain providing a conditioning environment for permeating ions and channel blockers. Indeed, in NMDAR channels, the M3 segment represents a critical element mediating the high Ca^{2+} influx (Watanabe et al., in press) and binding of open channel blockers (Fig. 5, Sobolevsky et al., 2002; Kashiwagi et al., 2002). The contribution of the NR1 and NR2 subunits to these processes, however, is not equivalent. Negative charges in the NR1 M3 segment, for example, mediate the high Ca^{2+} influx, whereas homologous ones in NR2A make little or no contribution to this process. This difference between the subunits may in part reflect the asymmetrical positioning of subunits. Hence, polar and charged residues in NR1, because they are positioned deeper in the pore than homologous ones in NR2, may exert a greater influence on permeation mechanisms.

Is staggering of subunits a general structural principle in all GluR subtypes? In contrast to NMDARs, AMPA and kainate receptors can form homomultimers as well as heteromultimers, and are activated by the single agonist, glutamate. Homomeric AMPA receptors also show a fourfold gating symmetry, suggesting an equivalence of subunits (Rosenmund et al., 1998; Robert et al., 2001) arguing against any structural asymmetry. However, vertically shifted transmembrane domains could represent a physical mechanism for the selective assembly of heterodimers, with identical subunits positioned on the opposite sides of the channel pore (Mansour et al., 2001). Indeed, the assembly of heteromeric structures depends on the compatibility of the membrane domains (Ayalon and Stern-Bach, 2001). Nevertheless, the relevance of subunit staggering in homomeric and heteromeric non-NMDAR channels remains unknown.

REFERENCES

Amar, M., F. Perin-Dureau, and J. Neyton. 2001. High-affinity Zn block in recombinant *N*-methyl-D-aspartate receptors with cysteine substitutions at the Q/R/N site. *Biophys. J.* 81:107–116.

Anson, L. C., P. E. Chen, D. J. Wyllie, D. Colquhoun, and R. Schoepfer. 1998. Identification of amino acid residues of the NR2A subunit that control glutamate potency in recombinant NR1/NR2A NMDA receptors. *J. Neurosci.* 18:581–589.

Antonov, S. M., V. E. Gmiro, and J. W. Johnson. 1998. Binding sites for permeant ions in the channel of NMDA receptors and their effects on channel block. *Nat. Neurosci.* 1:451–461.

Ayalon, G., and Y. Stern-Bach. 2001. Functional assembly of AMPA and kainate receptors is mediated by several discrete protein-protein interactions. *Neuron.* 31:103–113.

Banke, T. G., and S. F. Traynelis. 2001. Gating kinetics of individual NMDA receptors studied in excised membrane patches. *Soc. Neurosci. Abstr.* 703:6.

Beck, C., L. P. Wollmuth, P. H. Seeburg, B. Sakmann, and T. Kuner. 1999. NMDAR channel segments forming the extracellular vestibule inferred from the accessibility of substituted cysteines. *Neuron.* 22:559–570.

Benveniste, M., and M. L. Mayer. 1995. Trapping of glutamate and glycine during open channel block of rat hippocampal neuron NMDA receptors by 9-aminoacridine. *J. Physiol.* 483:367–384.

Burnashev, N., R. Schoepfer, H. Monyer, J. P. Ruppersberg, W. Gunther, P. H. Seeburg, and B. Sakmann. 1992. Control by asparagine residues of calcium permeability and magnesium blockade in the NMDA receptor. *Science.* 257:1415–1419.

Chatterton, J. E., M. Awobuluyi, L. S. Premkumar, H. Takahashi, M. Talantova, Y. Shin, J. Cui, S. Tu, K. A. Sevarino, N. Nakanishi, G. Tong, S. A. Lipton, and D. Zhang. 2002. Excitatory glycine receptors containing the NR3 family of NMDA receptor subunits. *Nature.* 415: 793–798.

Chiamvimonvat, N., M. T. Perez-Garcia, R. Ranjan, E. Marban, and G. F. Tomaselli. 1996. Depth asymmetries of the pore-lining segments of the Na^+ channel revealed by cysteine mutagenesis. *Neuron.* 16:1037–1047.

Dingledine, R., K. Borges, D. Bowie, and S. F. Traynelis. 1999. The glutamate receptor ion channels. *Pharmacol. Rev.* 51:7–61.

Doyle, D. A., J. Morais Cabral, R. A. Pfuetzner, A. Kuo, J. M. Gulbis, S. L. Cohen, B. T. Chait, and R. MacKinnon. 1998. The structure of the potassium channel: molecular basis of K^+ conduction and selectivity. *Science.* 280:69–77.

Hirai, H., J. Kirsch, B. Laube, H. Betz, and J. Kuhse. 1996. The glycine binding site of the *N*-methyl-D-aspartate receptor subunit NR1: identification of novel determinants of co-agonist potentiation in the extracellular M3–M4 loop region. *Proc. Natl. Acad. Sci. U.S.A.* 93:6031–6036.

Hollmann, M., and S. Heinemann. 1994. Cloned glutamate receptors. *Annu. Rev. Neurosci.* 17:31–108.

Holm, R. H., P. Kennepohl, and E. I. Solomon. 1996. Structural and functional aspects of metal sites in biology. *Chem. Rev.* 96:2239–2314.

Horenstein, J., D. A. Wagner, C. Czajkowski, and M. H. Akabas. 2001. Protein mobility and GABA-induced conformational changes in GABA(A) receptor pore-lining M2 segment. *Nat. Neurosci.* 4:477–485.

Jones, K. S., H. M. VanDongen, and A. M. VanDongen. 2002. The NMDA receptor M3 segment is a conserved transduction element coupling ligand binding to channel opening. *J. Neurosci.* 22:2044–2053.

Karlin, A. 2002. Emerging structure of the nicotinic acetylcholine receptors. *Nat. Rev. Neurosci.* 3:102–114.

Karlin, A., and M. H. Akabas. 1998. Substituted-cysteine accessibility method. *Methods Enzymol.* 293:123–145.

Kashiwagi, K., T. Masuko, C. D. Nguyen, T. Kuno, I. Tanaka, K. Igarashi, and K. Williams. 2002. Channel blockers acting at *N*-methyl-D-aspartate receptors: differential effects of mutations in the vestibule and ion channel pore. *Mol. Pharmacol.* 61:533–545.

Kohda, K., Y. Wang, and M. Yuzaki. 2000. Mutation of a glutamate receptor motif reveals its role in gating and delta2 receptor channel properties. *Nat. Neurosci.* 3:315–322.

Krupp, J. J., B. Vissel, S. F. Heinemann, and G. L. Westbrook. 1998. N-terminal domains in the NR2 subunit control desensitization of NMDA receptors. *Neuron.* 20:317–327.

Kuner, T., L. P. Wollmuth, A. Karlin, P. H. Seeburg, and B. Sakmann. 1996. Structure of the NMDA receptor channel M2 segment inferred from the accessibility of substituted cysteines. *Neuron.* 17:343–352.

Kuryatov, A., B. Laube, H. Betz, and J. Kuhse. 1994. Mutational analysis of the glycine-binding site of the NMDA receptor: structural similarity with bacterial amino acid-binding proteins. *Neuron.* 12:1291–1300.

Laube, B., H. Hirai, M. Sturgess, H. Betz, and J. Kuhse. 1997. Molecular determinants of agonist discrimination by NMDA receptor subunits: analysis of the glutamate binding site on the NR2B subunit. *Neuron.* 18:493–503.

Leszkiewicz, D. N., K. Kandler, and E. Aizenman. 2000. Enhancement of NMDA receptor-mediated currents by light in rat neurones in vitro. *J. Physiol.* 524:365–374.

Liu, Y., M. Holmgren, M. E. Jurman, and G. Yellen. 1997. Gated access to the pore of a voltage-dependent K$^+$ channel. *Neuron.* 19:175–184.

Liu, Y., M. E. Jurman, and G. Yellen. 1996. Dynamic rearrangement of the outer mouth of a K$^+$ channel during gating. *Neuron.* 16:859–867.

Loring, R. H., Y. M. Dou, W. Lane, G. S. Jones, Jr., and K. J. Stevenson. 1992. Aromatic trivalent arsenicals: covalent yet reversible reagents for the agonist binding site of nicotinic receptors. *Mol. Brain Res.* 15:113–120.

Mansour, M., N. Nagarajan, R. B. Nehring, J. D. Clements, and C. Rosenmund. 2001. Heteromeric AMPA receptors assemble with a pre-ferred subunit stoichiometry and spatial arrangement. *Neuron.* 32:841–853.

Paoletti, P., and P. Ascher. 1994. Mechanosensitivity of NMDA receptors in cultured mouse central neurons. *Neuron.* 13:645–655.

Robert, A., S. N. Irizarry, T. E. Hughes, and J. R. Howe. 2001. Subunit interactions and AMPA receptor desensitization. *J. Neurosci.* 21:5574–5586.

Rosenmund, C., Y. Stern-Bach, and C. F. Stevens. 1998. The tetrameric structure of a glutamate receptor channel. *Science.* 280:1596–1599.

Sillen, L. G., and A. E. Martell. 1964. Stability Constants of Metal-Ion Complexes. Special Publication No. 17. The Chemical Society, London.

Sobolevsky, A. I. 1999. Two-component blocking kinetics of open NMDA channels by organic cations. *Biochim. Biophys. Acta.* 1416:69–91.

Sobolevsky, A. I., C. Beck, and L. P. Wollmuth. 2002. Molecular rearrangements of the extracellular vestibule in NMDAR channels during gating. *Neuron.* 33:75–85.

Sobolevsky, A., and S. Koshelev. 1998. Two blocking sites of amino-adamantane derivatives in open *N*-methyl-D-aspartate channels. *Biophys. J.* 74:1305–1319.

Sobolevsky, A. I., S. G. Koshelev, and B. I. Khodorov. 1999. Probing of NMDA channels with fast blockers. *J. Neurosci.* 19:10611–10626.

Solomon, E. I., U. M. Sundaram, and T. E. Machonkin. 1996. Multicopper oxidases and oxygenases. *Chem. Rev.* 96:2563–2606.

Sprengel, R., R. Aronoff, M. Volkner, B. Schmitt, R. Mosbach, and T. Kuner. 2001. Glutamate receptor channel signatures. *Trends Pharmacol. Sci.* 22:7–10.

Subramaniam, S., S. D. Donevan, and M. A. Rogawski. 1994. Hydrophobic interactions of n-alkyl diamines with the *N*-methyl-D-aspartate receptor: voltage-dependent and -independent blocking sites. *Mol. Pharmacol.* 45:117–124.

Trower, M. K. 1996. In Vitro Mutagenesis Protocols, Vol. 57. Humana Press, Totowa, New Jersey.

Villarroel, A., M. P. Regalado, and J. Lerma. 1998. Glycine-independent NMDA receptor desensitization: localization of structural determinants. *Neuron.* 20:329–339.

Vissel, B., J. J. Krupp, S. F. Heinemann, and G. L. Westbrook. 2002. Intracellular domains of NR2 alter calcium-dependent inactivation of *N*-methyl-D-aspartate receptors. *Mol. Pharmacol.* 61:595–605.

Vlachova, V., H. Zemkova, and L. Vyklicky, Jr. 1996. Copper modulation of NMDA responses in mouse and rat cultured hippocampal neurons. *Eur. J. Neurosci.* 8:2257–2264.

Wollmuth, L. P., T. Kuner, and B. Sakmann. 1998. Intracellular Mg^{2+} interacts with structural determinants of the narrow constriction contributed by the NR1-subunit in the NMDA receptor channel. *J. Physiol.* 506:33–52.

Wollmuth, L. P., T. Kuner, P. H. Seeburg, and B. Sakmann. 1996. Differential contribution of the NR1- and NR2A-subunits to the selectivity filter of recombinant NMDA receptor channels. *J. Physiol.* 491:779–797.

Yang, J., P. T. Ellinor, W. A. Sather, J. F. Zhang, and R. W. Tsien. 1993. Molecular determinants of Ca^{2+} selectivity and ion permeation in L-type Ca^{2+} channels. *Nature.* 366:158–161.